Hindawi
Advances in Materials Science and Engineering
Volume 2022, Article ID 2869225, 11 pages
https://doi.org/10.1155/2022/2869225

Research Article

Influence of Planetary Ball Mill Parameters on Powder Flowability of AlSi10Mg with Niobium Carbide Using Central Composite Design (CCD)

Raj Mohan R,[1] **Venkatraman R**,[1] **Raghuraman S**,[1] **Manoj Kumar P**,[2] **Rajneesh Sharma**,[3] **Ankit**,[4] **Atul Sarojwal**,[5] **and Rajkumar S**[6]

[1]*School of Mechanical Engineering, SASTRA Deemed to Be University, Thanjavur 613401, Tamil Nadu, India*
[2]*Department of Mechanical Engineering, KPR Institute of Engineering and Technology, Coimbatore 641407, Tamil Nadu, India*
[3]*Department of Civil Engineering, Government Engineering College, Jhalawar 326023, Rajasthan, India*
[4]*Department of Mechanical Engineering, Government Engineering College, Jhalawar 326023, Rajasthan, India*
[5]*Department of Electrical Engineering, FET, MJP Rohilkhand University, Bareilly 243006, UP, India*
[6]*Department of Mechanical Engineering, Faculty of Manufacturing, Institute of Technology, Hawassa University, Hawassa, Ethiopia*

Correspondence should be addressed to Rajkumar S; rajkumar@hu.edu.et

Received 13 April 2022; Accepted 7 July 2022; Published 3 August 2022

Academic Editor: Adel Mohamed

The hypoeutectic aluminum alloy (AlSi10Mg) is a well-known candidate material used predominantly for its processability and inherent characteristics in metal-based additive manufacturing. Besides, transition metal carbide, such as niobium carbide (NbC), is added to the AlSi10Mg, enhancing its mechanical properties and preferably its wear resistance to the matrix. However, in additive manufacturing, the mixed powder's flowability is a prerequisite for determining the final properties of the specimens. In this study, mixed powder flowability analysis was carried out through the regular mixing of AlSi10Mg with a varying weight percentage of NbC conducted in the planetary ball mill with different time, speed, and NbC composition following the Central Composite Design (CCD), with a total of 20 experiments. Here, regular mixing was preferred to retain the morphology of the AlSi10Mg (spherical shape) instead of ball milling, which contributes to the degradation of the powder's shape and size. Finally, based on the combined analysis of apparent density (AD), tapped density (TD), and static angle of repose (SAoR), the flowability characteristics of the mixed powders (AlSi10Mg + X % NbC) were evaluated. The optimum combination (AlSi10Mg + X% NbC) was attained based on the composite desirability criteria.

1. Introduction

Metal-based additive manufacturing is an emerging technology that produces components within the stipulated period and achieves high dimensional accuracy [1]. Generally, this technology employs only a specified powder category, such as atomized particles, depending on the manufacturer's specification. The atomized powder properties must be addressed based on the processability criterion to ensure the component's print quality [2]. The properties of the powder comprise the flowability, the density of the powder (apparent density and tapped density), particle shape (morphology), the powder synthesis process, and the particle size distribution (PSD) that affect the building of the powder layer on the platform. The flowability of the powder should be adequate for an effective additive manufacturing process [3]. In processing aluminum alloys by additive manufacturing, the powder's morphology and size distribution play a decisive role in ensuring the material's packing density [4]. The particle shape significantly influences good flowability than the size distribution [5]. Ball milling is widely preferred for aluminum-based matrix

composites to mix/blend the two different sizes and shapes of powders (matrix + reinforcement) in varying volumes or weight percentages following other optimization techniques.

Moreover, the ball mill's input parameters substantially affect the blended powder flow properties [6–14]. For the application of greater hardness, niobium carbide (NbC) is preferred among other transition metal carbides (TMC) due to its higher bulk modulus and incorporating an irregular-shaped carbide as reinforcement improves the wear resistance of the matrix element [15, 16]. The mixing of two different powders (metals as matrix and ceramic as reinforcement) with various morphologies was possible to process through casting [17] and powder metallurgy [18] routes for powder preparation. Compared to the previous routes, ceramic reinforcements (other TMCs) in the Al-based matrix showed remarkable mechanical properties such as high hardness and high wear resistance [19] when compared to the base alloy through the selective laser melting (SLM) process and are suitable for tribological applications. Furthermore, compared to traditional approaches such as casting and powder metallurgy, composite fabrication via additive manufacturing has benefits in terms of design, freedom, and the ability to manufacture complicated designs [20]. However, it is challenging because of the additive manufacturing processability [21].

From a critical review of the literature, it was noted that the optimization of powder flow characteristics in the combination of hypoeutectic aluminum alloy (AlSi10Mg) and group VB transition metal carbide (NbC) was not explored much in the scope of additive manufacturing. Therefore, evaluating the mixed powder characteristics of AlSi10Mg (spherical) and NbC (aggregate irregular) with varying weight percentages is required before being fed into the processing window of additive manufacturing. The objective of the work is to investigate the powder flowability characteristics of AlSi10Mg with the addition of NbC based on apparent density (AD), tapped density (TD), and static angle of repose (SAoR) values through regular mixing in a planetary ball mill following the central composite design approach. At the same time, the Hausner's Ratio (HR) and the Carr Index (CI) values resulted from the apparent and tapped densities of the mixed powder.

2. Materials and Methods

The AlSi10Mg powder (Si–10; Mg–0.35; Al-Balance; Supplier: Carpenter Additive, UK) of a mean particle size of 41.79 microns and NbC powder (99% Pure; Supplier: Alfa Aesar, UK) of a mean particle size of 12.05 microns were used. The AlSi10Mg was considered a matrix element in the experimental study, whereas the NbC was taken as particulate ceramic reinforcement. The morphology of procured AlSi10Mg with a spherical shape and NbC with an aggregate irregular shape was observed using a scanning electron microscope (Vega3 TESCAN) analysis, as shown in Figures 1(a) and 1(b). The X-ray photoelectron spectroscope (Thermo Fisher) analysis was carried out for procured powders, as shown in Figure 2, and no impurities were identified in either of the powder samples. Two powders were regularly mixed using a planetary ball mill with a single jar holder (VB Ceramic Consultants, India). For maintaining the spherical shape of the AlSi10Mg, the balls are not used during regular mixing. Using MINITAB (Version-18.0), the central composite design (CCD) was preferred in this investigation to analyze and optimize the planetary ball mill's input parameters to ensure the effects of extreme levels of factors involved. The three main input parameters for regular mixing using a planetary ball mill are time (hours), speed (RPM), and NbC composition (% weight), which play a vital role in predicting powder flowability. The input parameters and levels are shown in Table 1. Based on the three input factors and five levels of each factor, 20 sets of experiments were designed and included in Table 2. The scanning electron microscope (SEM) samples examined the morphology change of the master alloy and ensured the distribution of reinforcement in the matrix. The powder flow characteristics study was performed based on apparent density: ASTM B 212, tapped density: ASTM B 527 [22], static angle of repose: ASTM B213 [23], Hausner's Ratio: ASTM D7481-09, and Carr Index: ASTM D6393-14 [24].

3. Results and Discussion

3.1. Analysis of CCD Experiments. The CCD was employed to predict the influence of the extreme limits of the input parameters such as time, speed, and composition on the output responses. Also, CCD was used for developing the mathematical model for the responses such as apparent density, tapped density, and static angle of repose. The apparent density and tapped density values were obtained by the Hall flowmeter method and mechanical tapping 50 times, respectively, conforming to the ASTM standards. Generally, the lower values of apparent and tapped densities exhibit the poor flowability of the powders. For the flowability indication of mixed powder, the HR and CI values were attained using (1) and (2). For better flowability, the lower Hausner's Ratio and Carr Index values were preferred. The static angle of repose of the mixed powder was attained using (3) based on the piling diameter and height, followed by the fixed cone height approach. The static angle of repose was used to assess the mixed powder's internal condition, such as cohesiveness or friction between the particles. More cohesiveness leads to an increased static angle of repose and affects the flow of the mixed powder. Table 3 shows the data of output responses based on the CCD experiments. In experimental analysis, the CCD experiments were classified into three categories, namely , center-based (E5, E6, E11, E18, E19, and E20), extreme-based (E3, E4, E9, E13, E16, and E17), and factor-based (E1, E2, E7, E8, E10, E12, E14, and E15). From Table 3, it was noted that experiments E4 and E9 show the worst flow characteristics based on the results of the output responses due to the mixing in extreme conditions like a more extended time (6.02 hours) and higher NbC composition (11.043% weight) under the rotational speed of 150 RPM.

Conversely, E8, E10, E12, E13, E14, and E15 show good flowability of mixed powders based on the lower HR, CI, and SAoR. The remaining experiments, E1, E2, E3, E5, E6,

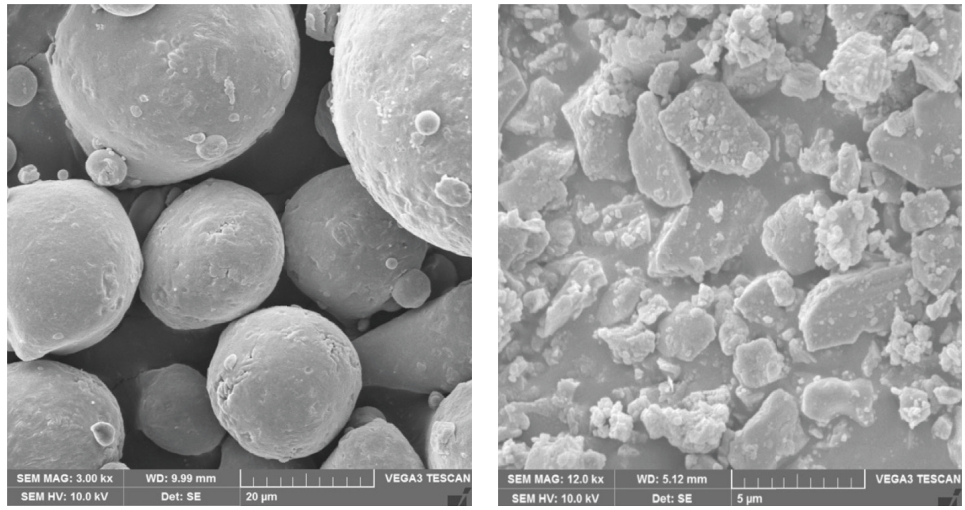

(a) (b)

Figure 1: Morphology of (a) AlSi10Mg and (b) NbC.

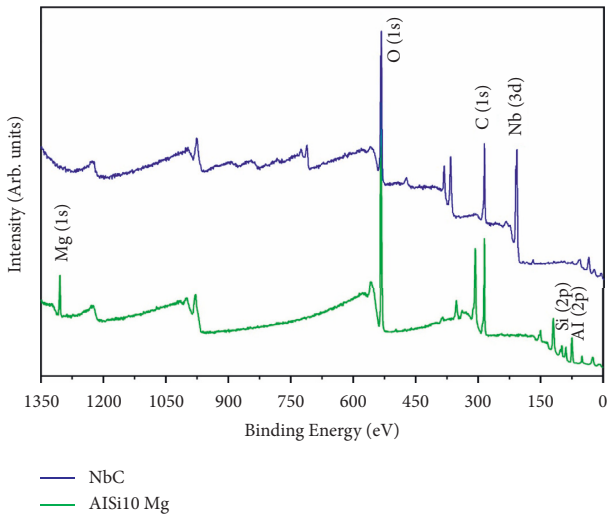

Figure 2: XPS spectra of AlSi10Mg and NbC.

Table 1: Input parameters and their levels for regular mixing.

Input parameters	Levels				
	$-\alpha$	−1	0	1	$+\alpha$
Time (hours): A	0.98	2	3.5	5	6.02
Speed (RPM): B	65.95	100	150	200	234.05
NbC composition (% weight): C	0.957	3	6	9	11.043

E7, E11, E16, E17, E18, E19, and E20, exhibit fair flow characteristics. From the observations, irrespective of varying NbC composition, it was clear that the factor-based experiments yielded a good flow for the mixed powders

Table 2: CCD experiment design with factors.

Experiment no.	A	B	C
E1	2	200	3
E2	5	200	9
E3	0.98	150	6
E4	3.5	150	11.043
E5	3.5	150	6
E6	3.5	150	6
E7	5	200	3
E8	2	100	3
E9	6.02	150	6
E10	5	100	9
E11	3.5	150	6
E12	5	100	3
E13	3.5	234.05	6
E14	2	200	9
E15	2	100	9
E16	3.5	65.95	6
E17	3.5	150	0.957
E18	3.5	150	6
E19	3.5	150	6
E20	3.5	150	6

owing to the proper set of input parameters, except for E1, E2, and E7. These experiments also exhibit good HR and CI, but the angle of repose is high due to the nonuniform dispersion of NbC particles, affecting the flow and inducing a frictional effect between the reinforcement and matrix. Moreover, the center-based and extreme-based experiments do not yield satisfactory results, except for experiment E13, because the mixing occurs at a higher speed of 234.05 RPM.

Table 3: Output responses based on CCD-based experiments.

Experiment no.	Apparent density (g/cc)	Tapped density (g/cc)	Static angle of repose (Radian)	Hausner's Ratio (no unit)>	Carr Index (%)
E1	1.140	1.359	0.547	1.19	16.14
E2	1.270	1.529	0.567	1.20	16.94
E3	1.258	1.522	0.531	1.21	17.33
E4	1.284	1.608	0.597	1.25	20.15
E5	1.251	1.545	0.510	1.23	19.02
E6	1.251	1.545	0.540	1.23	19.02
E7	1.161	1.375	0.516	1.18	15.58
E8	1.234	1.470	0.479	1.19	16.05
E9	1.242	1.603	0.597	1.29	22.53
E10	1.292	1.531	0.486	1.18	15.59
E11	1.251	1.555	0.528	1.24	19.52
E12	1.276	1.507	0.440	1.18	15.33
E13	1.187	1.334	0.489	1.12	11.04
E14	1.280	1.486	0.488	1.16	13.89
E15	1.333	1.537	0.448	1.15	13.28
E16	1.310	1.601	0.389	1.22	18.18
E17	1.153	1.409	0.542	1.22	18.17
E18	1.251	1.545	0.528	1.23	19.02
E19	1.251	1.545	0.528	1.23	19.02
E20	1.251	1.545	0.528	1.23	19.02

$$\text{Hausner's Ratio}\,(HR) = \frac{\text{Tapped Density}}{\text{Apparant Density}}, \tag{1}$$

$$\text{Carr Index}\,(CI) = \frac{\text{Tapped Density} - \text{Apparant Density}}{\text{Tapped Density}} \times 100, \tag{2}$$

$$\text{Static Angle of Repose}\,(SAoR),\ \tan\theta = \frac{2 \times \text{Height of the Piling}\ (H\ in\ mm)}{\text{Base Diameter of the Piling}\ (D\ in\ mm)}. \tag{3}$$

The center-based, extreme-based, and factor-based scanning electron microscope (SEM) images are shown in Figures 3–5, respectively. The SEM images of the mixed powder under various input parameters were used to ensure the morphology of the AlSi10Mg with NbC and the distribution of the reinforcement (NbC) in the matrix (AlSi10Mg). Figures 3–5 depict that the AlSi10Mg morphology is not modified, and NbC particles' presence was observed. Here, the yellow circle is used to indicate the presence of NbC particles in the matrix.

3.2. Percentage Contribution of Input Parameters for Responses. Table 4shows the statistical values based on the full quadratic model. The values depict that the model is adequate for analysis and further experimentation. If the p value and F-value are less than 0.05 and greater than 4, respectively, at a 95 percent confidence level, the proposed model is significant, and the corresponding input parameter is taken into account for the output response. The model's R square value for all responses was greater than 90 percent, which reveals that the model could explore 90 percent of the possible changes in the output responses. The model can significantly predict the process if the R square and adjusted R square values are greater than 80 percent. The input parameters, such as speed and NbC composition, contribute more substantially to the responses, such as apparent density and tapped density. The most vital input parameter affecting the static angle of repose is speed. Also, the interaction of time and NbC composition contributes to the static angle of repose.

3.3. Validation of Regression Equation. The regression equations (4)–(6) were used to predict output responses such as apparent density, tapped density, and static angle of repose by including quadratic terms of linear, square, and two-way interaction of input parameters. The residual value was obtained from the difference between experimented and predicted data. If the residual values are small, the proposed regression equations are accurate. Table 5 shows the residual values for the responses, depicting that the fitted data are close to the experimented data. So, the proposed regression equations have verified the adequacy of the full quadratic model.

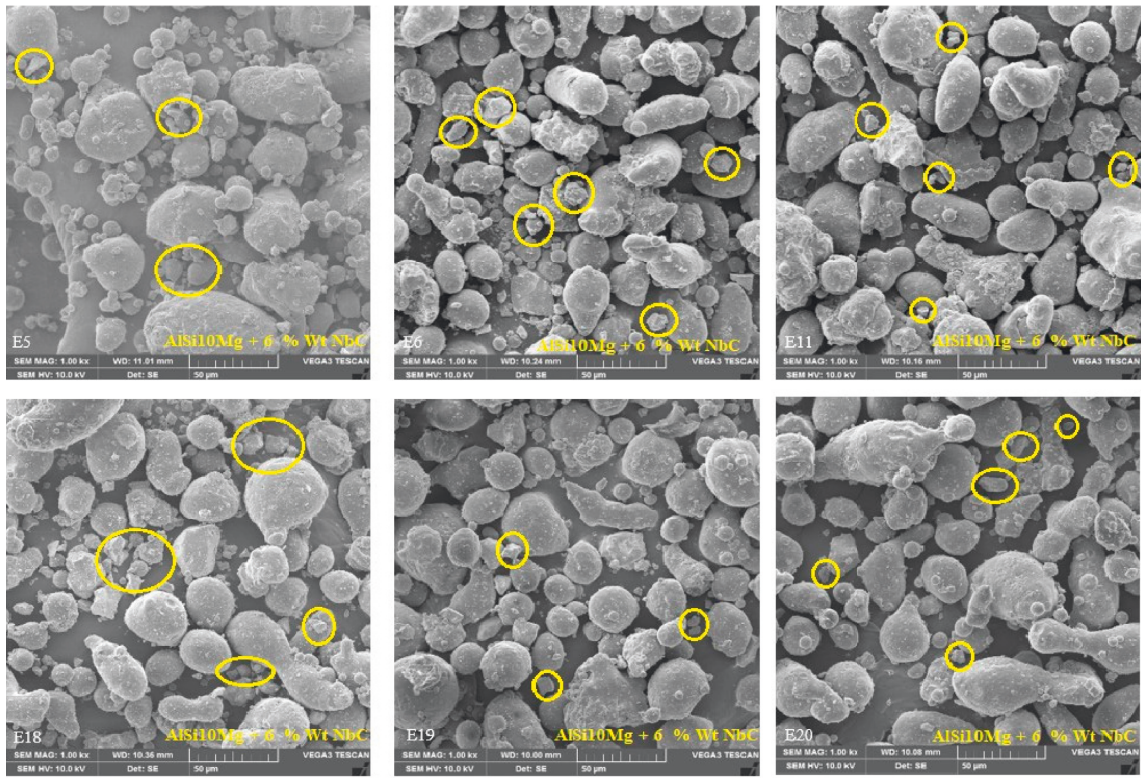

Figure 3: SEM images of center-based experiments.

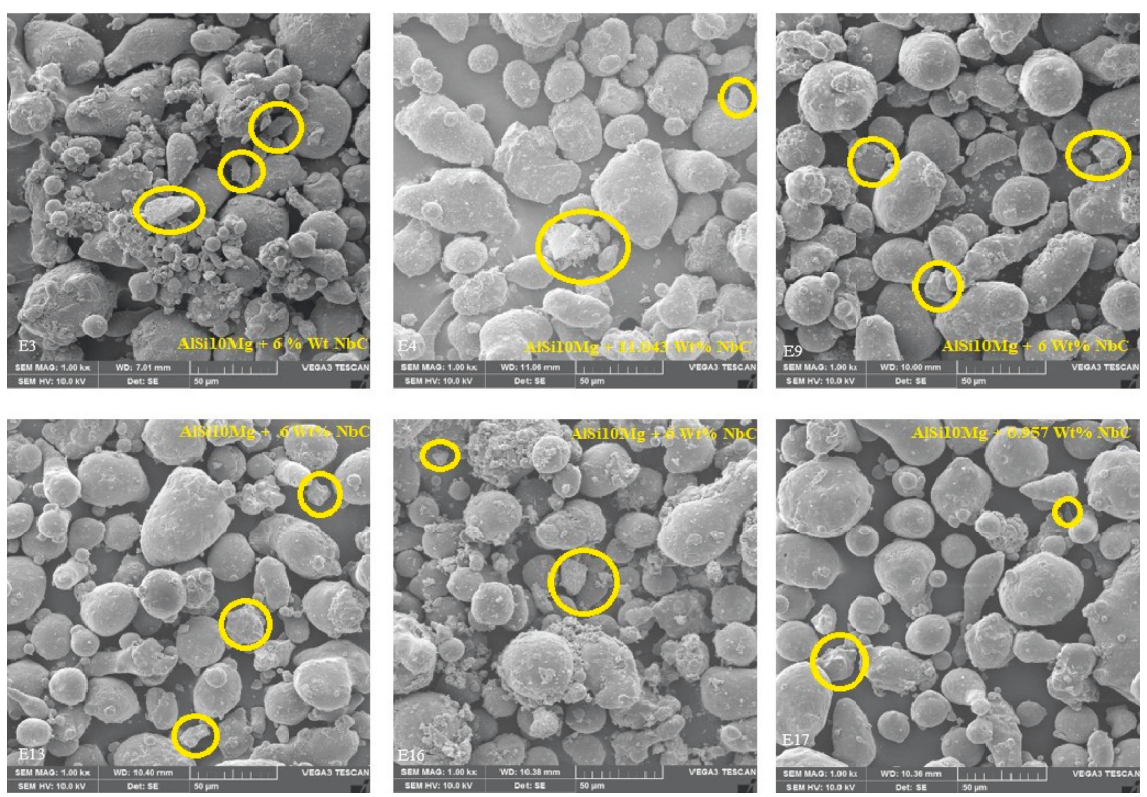

Figure 4: SEM images of extreme-based experiments.

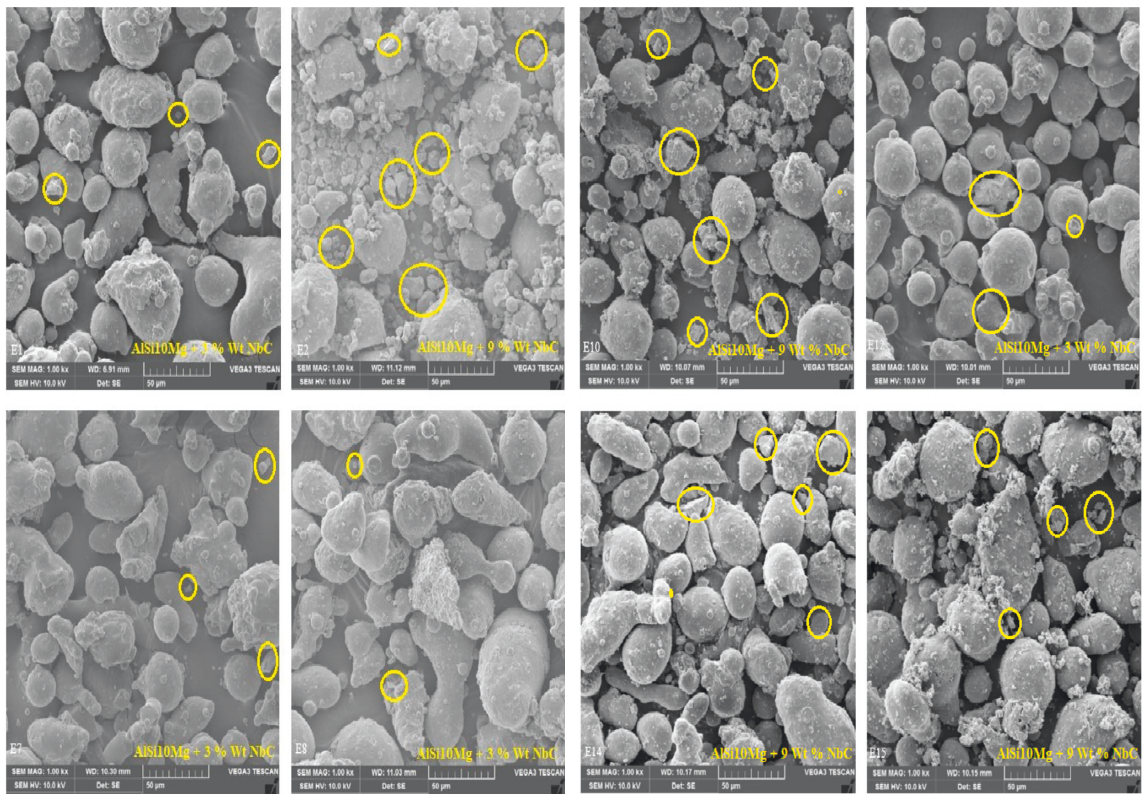

Figure 5: SEM images of factor-based experiments.

Table 4: Analysis of variance and contribution of input parameters.

Source	Input parameters: time (A); speed (B); NbC composition (C) Responses: apparent density (R1); tapped density (R2); static angle of repose (R3) Adjusted sum of squares			*p* value			*F*-value			% contribution to input parameters (calculation error: ±1%)		
	R1	R2	R3	R1	R2	R3	R1	R2	R3	R1	R2	R3
Model	0.048	0.109	0.044	≤0.001	0.001	≤0.001	57.26	10.07	10.91			
Linear	0.043	0.081	0.016	≤0.001	≤0.001	0.001	152.7	22.49	11.95			
A	0.000	0.004	0.002	0.694	0.107	0.074	0.16	3.13	3.99	0.03	3.11	3.69
B	0.018	0.041	0.014	≤0.001	≤0.001	≤0.001	190.4	33.90	30.23	36.26	33.68	27.94
C	0.025	0.037	0.001	≤0.001	≤0.001	0.231	267.7	30.44	1.63	50.96	30.24	1.50
Square	0.001	0.023	0.023	0.021	0.011	≤0.001	5.14	6.44	17.31			
A*A	0.000	0.000	0.001	0.528	0.819	0.232	0.43	0.06	1.62	0.08	0.05	1.50
B*B	0.000	0.019	0.020	0.706	0.003	≤0.001	0.15	15.42	43.70	0.03	15.32	40.38
C*C	0.001	0.006	0.001	0.004	0.042	0.137	13.90	5.40	2.61	2.65	5.37	2.42
2-way interaction	0.004	0.005	0.005	0.001	0.331	0.058	13.86	1.29	3.49			
A*B	0.000	0.000	0.000	0.717	0.781	0.436	0.14	0.08	0.66	0.03	0.08	0.61
A*C	0.002	0.000	0.004	0.002	0.869	0.011	17.34	0.03	9.65	3.30	0.03	8.91
B*C	0.002	0.005	0.000	0.001	0.081	0.706	24.10	3.76	0.15	4.59	3.74	0.14
Error	0.001	0.012	0.005							1.90	9.94	9.24
Total	0.049	0.121	0.049									
R square	98.10%	90.06%	90.76%									
R square (adj.)	96.38%	81.12%	82.45%									

Table 5: Validation of regression equation.

Run order	Predicted (P) vs. experimented (E)								
	Apparent density (g/cc)			Tapped density (g/cc)			Static angle of repose (radian)		
	p	*E*	Residue	*p*	*E*	Residue	*p*	*E*	Residue
E1	1.134	1.140	0.006	1.337	1.359	0.022	0.540	0.547	0.007
E2	1.254	1.270	0.016	1.528	1.529	0.001	0.584	0.567	−0.017
E3	1.258	1.258	0.000	1.514	1.522	0.008	0.529	0.531	0.002
E4	1.296	1.284	−0.012	1.575	1.608	0.033	0.566	0.597	0.031
E5	1.251	1.251	0.000	1.548	1.545	−0.003	0.528	0.510	−0.018
E6	1.251	1.251	0.000	1.548	1.545	−0.003	0.528	0.540	0.012
E7	1.163	1.161	−0.002	1.381	1.375	−0.006	0.529	0.516	−0.013
E8	1.242	1.234	−0.008	1.500	1.470	−0.030	0.483	0.479	−0.004
E9	1.254	1.242	−0.012	1.570	1.603	0.033	0.568	0.597	0.029
E10	1.290	1.292	0.002	1.583	1.531	−0.052	0.515	0.486	−0.029
E11	1.251	1.251	0.000	1.548	1.555	0.007	0.528	0.528	0.000
E12	1.266	1.276	0.010	1.531	1.507	−0.024	0.447	0.440	−0.007
E13	1.193	1.187	−0.006	1.355	1.334	−0.021	0.477	0.489	0.012
E14	1.282	1.280	−0.002	1.492	1.486	−0.006	0.502	0.488	−0.014
E15	1.323	1.333	0.010	1.560	1.537	−0.023	0.457	0.448	−0.009
E16	1.315	1.310	−0.005	1.539	1.601	0.062	0.370	0.389	0.019
E17	1.152	1.153	0.001	1.401	1.409	0.008	0.541	0.542	0.001
E18	1.251	1.251	0.000	1.548	1.545	−0.003	0.528	0.528	0.000
E19	1.251	1.251	0.000	1.548	1.545	−0.003	0.528	0.528	0.000
E20	1.251	1.251	0.000	1.548	1.545	−0.003	0.528	0.528	0.000

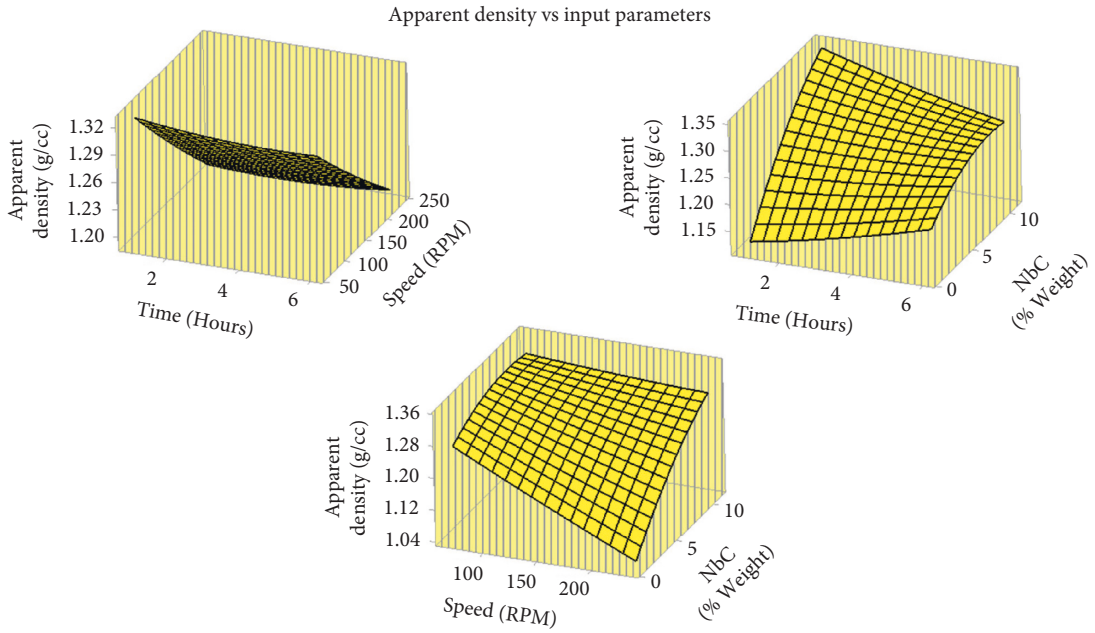

Figure 6: Surface plots for apparent density.

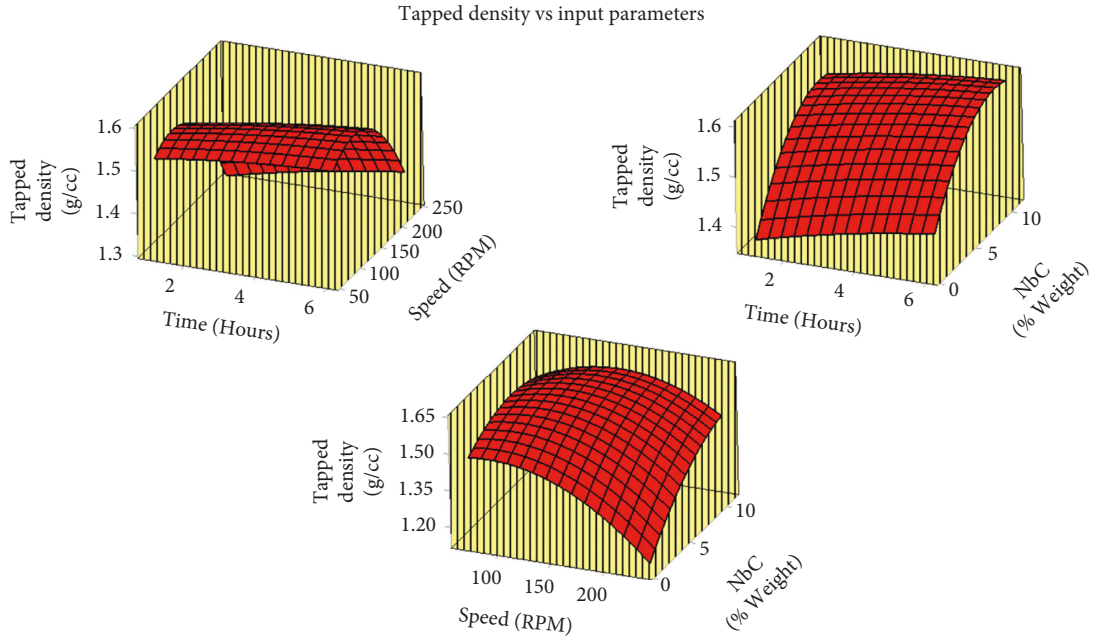

Figure 7: Surface plots for tapped density.

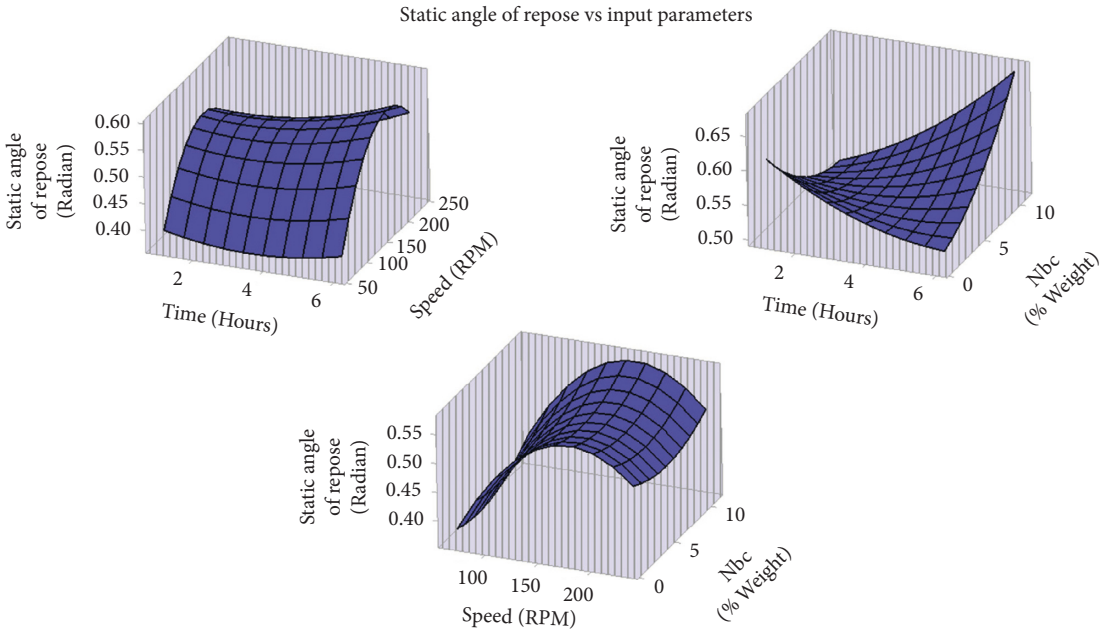

Figure 8: Surface plots for the static angle of repose.

Table 6: Criteria for composite desirability function.

Output response	Goal/objective	Lower value	Target	Upper value	Importance	Weight
Apparent density	Maximum	1.3340	1.6083	—	1	1
Tapped density	Maximum	1.1396	1.3330	—	1	1
Static angle of repose	Minimum	—	0.3892	0.597	1	1

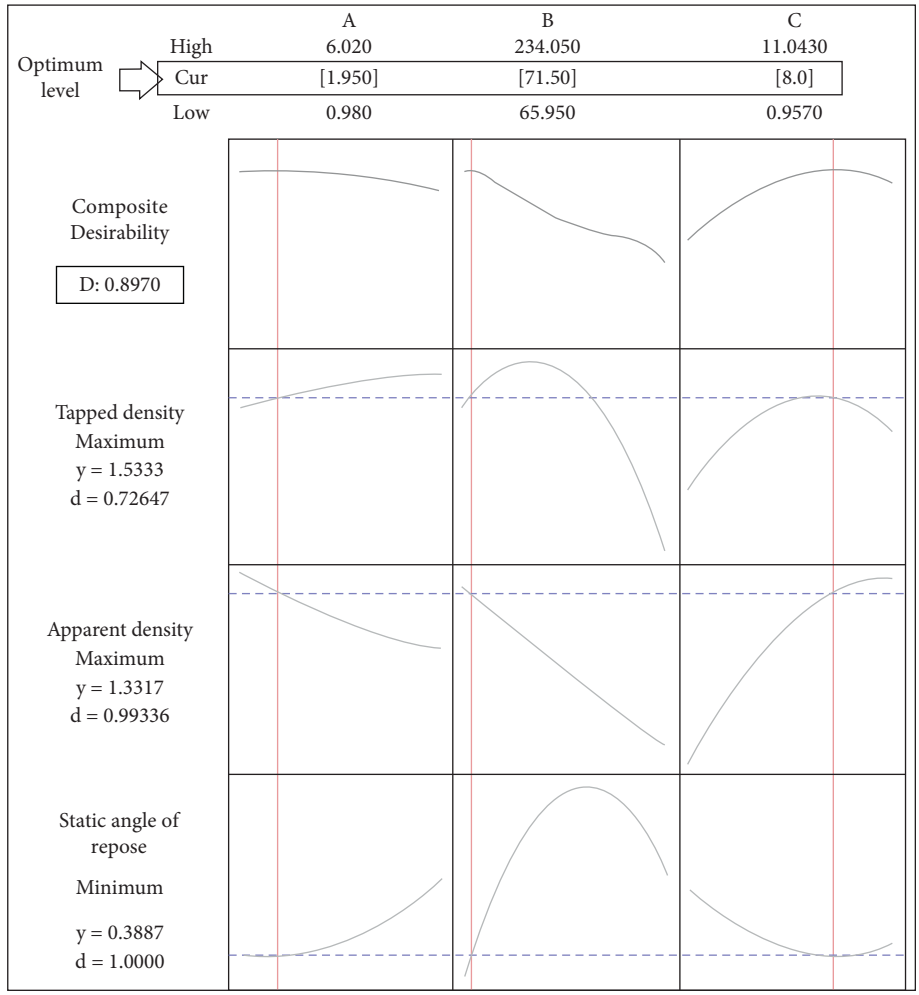

Figure 9: Composite desirability plot based on multiple responses.

$$\text{Apparent Density} = 1.2995 + 0.0105\,A - 0.00157\,B + 0.0212\,C + 0.00074\,AA + 0.000000\,BB - 0.00105\,CC + 0.000017\,AB - 0.00316\,AC + 0.000112\,BC, \tag{4}$$

$$\text{Tapped Density} = 1.3080 + 0.0135\,A + 0.00210\,B + 0.0234\,C - 0.00095\,AA - 0.000014\,BB - 0.00236\,CC + 0.000047\,AB - 0.00046\,AC + 0.000158\,BC, \tag{5}$$

$$\textit{Static Angle of Repose} = 0.2680 - 0.0579\,A - 0.00491\,B - 0.0249\,C + 0.00371\,AA - 0.000015\,BB + 0.01007\,CC + 0.000081\,AB + 0.00519\,AC - 0.000019\,BC \tag{6}$$

3.4. Surface Plots for the Output Responses. Based on the proposed and verified model, the 3D surface plots for apparent density, tapped density, and static angle of repose are generated and shown in Figures 6–8, respectively. It displays the influence of time versus speed, time versus NbC composition, and speed versus NbC composition on different output responses with fixed input parameters at the zero (coded) level. It is observed that the apparent density and tapped density decreased as the speed increased. In contrast, both the densities were increased as the NbC composition increased. At the lower mixing speed (less than 100 RPM) with a higher weight percentage of NbC, the apparent and tapped density values were high. So, the HR and CI values were high at the low-speed mixing. The static angle of repose decreases with decreasing speed. Irrespective of increasing the NbC composition, the value of the static angle of repose was minimum at a low speed of less than 100 RPM. Finally, time plays a less significant role in deciding the change in output responses.

3.5. Composite Desirability and Validation. The composite desirability function can achieve multiple response objectives/goals. Here, the objective is to attain a maximum apparent and

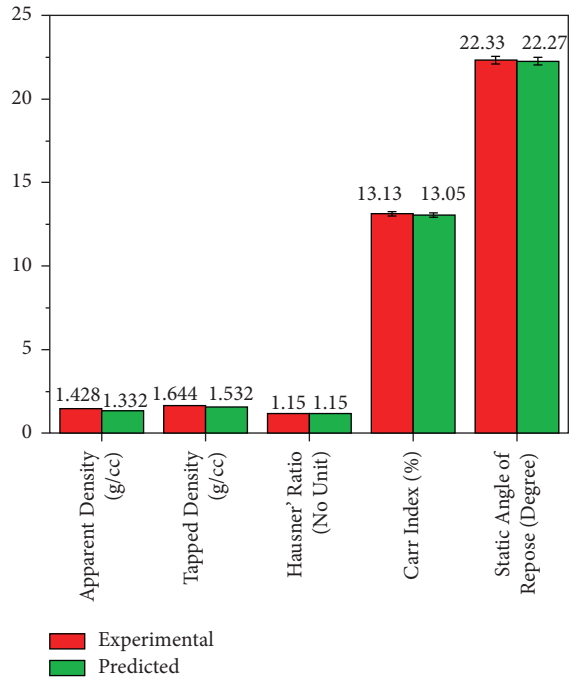

Figure 10: Comparison between experimental and predicted values for optimum conditions.

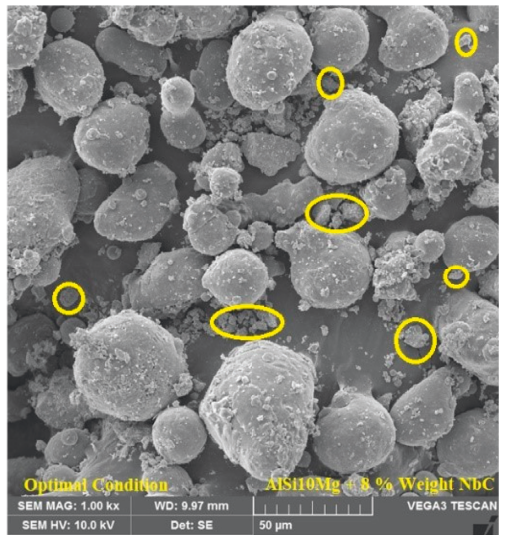

Figure 11: SEM image for the optimum combination of AlSi10Mg + 8% weight of NbC.

tapped densities with the minimum static angle of repose. The maximum apparent density ensures that the mixed powders are not entirely irregular in morphology, introduce smaller particles (NbC) between the AlSi10Mg particles, and have low pores in the initial packed density. The particles' cohesiveness was controlled, establishing good flow to the mixed powder at maximum tapped density criteria. Based on the maximum condition of both densities, low HR and CI were attained. These values ensure good flowability characteristics. Finally, the minimum static angle of repose confirms the low cohesiveness and minimum frictional effect during the powder flow. The static angle of repose is inversely proportional to the flowability of the mixed powder. Table 6 shows the goal of the output responses with importance and weight, along with constraint values.

Figure 9 displays the optimal results with a composite desirability limit to address the multiple objective output response by pulling out the higher and lower point from the 3D surface plot concerning the defined objective. The optimum condition is as follows: time = 1.95 hours, speed = 71.50 RPM, NbC composition = 8% weight. The predicted values of apparent density, tapped density, and static angle of repose are 1.3317 g/cc, 1.5333 g/cc, and 0.3887 radians (22.17 degrees) with composite desirability of 0.897.

As shown in Figure 10,the validation experiment was carried out under optimized conditions for the confirmatory purpose, and the experimental data were compared with predicted data, as shown in Figure 10. From Figure 11, it was observed that there was no change in the matrix (AlSi10Mg) morphology and tiny satellites on the surface of the matrix.

4. Conclusion

In this experimental investigation, the CCD was employed to predict the processing conditions for regular mixing of AlSi10Mg and NbC. From the experimental analysis, the following points can be observed:

(1) The factor-based experiments show promising results based on flowability characteristics when compared to center-based and extreme-based experiments

(2) Based on the SEM images, the morphology of the matrix element (AlSi10Mg) had not been changed after being mixed with varying percentages of NbC at a different set of parameters, and proper distribution of NbC was observed.

(3) The apparent and tapped density ratio was insufficient for predicting the flow of mixed powder. Another response is also required to assess the flow characteristics. So, the static angle of repose was employed to predict the mixed powder's cohesiveness despite its low HR and CI values. The undesired flow characteristics were observed at a high percentage of NbC and the extended mixing time.

(4) The optimum condition of input parameters reveals that the low-speed mixing was preferable to achieve maximum apparent and tapped densities with the minimum static angle of repose.

(5) Finally, the optimized combination of mixed powder (AlSi10Mg + 8% weight of NbC) was attained, showing good flowability characteristics. Furthermore, it satisfies the processability criteria of additive manufacturing.

Data Availability

The data used to support the findings of this study are included in the article.

Conflicts of Interest

The authors declare that there are no conflicts of interest regarding the publication of this paper.

Acknowledgments

This work was funded by the SASTRA Deemed to be University under Prof. T. R. Rajagopalan (TRR) Research Fund.

References

[1] G. Marchese, A. Aversa, M. Lorusso et al., "Development and characterisation of aluminium matrix nanocomposites AlSi10Mg/MgAl2O4 by laser powder bed fusion," *Metals*, vol. 8, no. 3, p. 175, 2018.

[2] J. Zegzulka, D. Gelnar, L. Jezerska, R. Prokes, and J. Rozbroj, "Characterization and flowability methods for metal powders," *Scientific Reports*, vol. 10, no. 1, Article ID 21004, 2020.

[3] A. B. Spierings, M. Voegtlin, T. Bauer, and K. Wegener, "Powder flowability characterisation methodology for powder-bed-based metal additive manufacturing," *Progress in Additive Manufacturing*, vol. 1, no. 1-2, pp. 9–20, 2016.

[4] R. Raj Mohan, R. Venkatraman, S. Raghuraman et al., "Processing of aluminium-silicon alloy with metal carbide as reinforcement through powder-based additive manufacturing: a critical study," *Scanning*, vol. 2022, pp. 1–14, 2022.

[5] K. Riener, N. Albrecht, S. Ziegelmeier et al., "Influence of particle size distribution and morphology on the properties of the powder feedstock as well as of AlSi10Mg parts produced by laser powder bed fusion (LPBF)," *Additive Manufacturing*, vol. 34, Article ID 101286, 2020.

[6] P. Ashwath and M. A. Xavior, "The effect of ball milling & reinforcement percentage on sintered samples of aluminium alloy metal matrix composites," *Procedia Engineering*, vol. 97, pp. 1027–1032, 2014.

[7] L. Kollo, M. Leparoux, C. R. Bradbury, C. Jäggi, E. Carreño-Morelli, and M. Rodríguez-Arbaizar, "Investigation of planetary milling for nano-silicon carbide reinforced aluminium metal matrix composites," *Journal of Alloys and Compounds*, vol. 489, no. 2, pp. 394–400, 2010.

[8] Y. Afkham, R. A. Khosroshahi, R. Kheirifard, R. T. Mousavian, and D. Brabazon, "Microstructure and morphological study of ball-milled metal matrix nanocomposites," *The Physics of Metals and Metallography*, vol. 118, no. 8, pp. 749–758, 2017.

[9] Q. Han, R. Setchi, and S. L. Evans, "Synthesis and characterisation of advanced ball-milled Al-Al2O3 nanocomposites for selective laser melting," *Powder Technology*, vol. 297, pp. 183–192, 2016.

[10] N. Senthil Kannan, R. Parameshwaran, P. T. Saravanakumar, P. M. Kumar, and M. L. Rinawa, "Performance and quality improvement in a foundry industry using fuzzy MCDM and lean methods," *Arabian Journal for Science and Engineering*, pp. 1–12, 2022.

[11] W. l. Gu, "Bulk Al/SiC nanocomposite prepared by ball milling and hot pressing method," *Transactions of Nonferrous Metals Society of China*, vol. 16, pp. s398–s401, 2006.

[12] V. Erturun and O. Sahin, "Investigation of microstructural evolution in ball-milling of SiC reinforced aluminum matrix composites," *Powder Metallurgy and Metal Ceramics*, vol. 57, no. 11-12, pp. 687–696, 2019.

[13] P. Kishore, P. M. Kumar, and D. Dinesh, "Wear analysis of Al 5052 alloy with varying percentage of tungsten carbide," *AIP Conference Proceedings*, vol. 2128, no. No. 1, 2019, July.

[14] P. Garg, A. Jamwal, D. Kumar, K. K. Sadasivuni, C. M. Hussain, and P. Gupta, "Advance research progresses in aluminium matrix composites: manufacturing & applications," *Journal of Materials Research and Technology*, vol. 8, no. 5, pp. 4924–4939, 2019.

[15] P. W. Muchiri, V. M. Mwalukuku, K. K. Korir, G. O. Amolo, and N. W. Makau, "Hardness characterization parameters of Niobium Carbide and Niobium Nitride: a first principles study," *Materials Chemistry and Physics*, vol. 229, pp. 489–494, 2019.

[16] M. Cuppari and S. Santos, "Physical properties of the NbC carbide," *Metals*, vol. 6, no. 10, p. 250, 2016.

[17] T. Satish Kumar, G. Suganya Priyadharshini, S. Shalini, K. Krishna Kumar, and R. Subramanian, "Characterization of NbC-reinforced AA7075 alloy composites produced using friction stir processing," *Transactions of the Indian Institute of Metals*, vol. 72, no. 6, pp. 1593–1596, 2019.

[18] D. N. Travessa, M. J. Silva, and K. R. Cardoso, "Niobium carbide-reinforced Al matrix composites produced by high-energy ball milling," *Metallurgical and Materials Transactions B*, vol. 48, no. 3, pp. 1754–1762, 2017.

[19] A. T. Ertürk, M. Şahin, and M. Aras, "Tribological behavior of SiC particulate reinforced AA5754 matrix composite under dry and lubricated conditions," *Transactions of the Indian Institute of Metals*, vol. 70, no. 5, pp. 1233–1240, 2017.

[20] A. T. Erturk, M. E. Bulduk, G. Tarakçi, G. Özer, and E. Yarar, "Investigation of the microstructure and mechanical characteristics of lattice structures produced by laser powder bed fusion method," *Metals and Materials International*, vol. 28, no. 1, pp. 155–167, 2022.

[21] Y. Li, D. Gu, H. Zhang, and L. Xi, "Effect of trace addition of ceramic on microstructure development and mechanical properties of selective laser melted AlSi10Mg alloy," *Chinese Journal of Mechanical Engineering*, vol. 33, no. 1, p. 33, 2020.

[22] J. W. Carson and B. H. Pittenger, "Bulk properties of powders, içinde," *ASM Handbook Volume*, vol. 7, pp. 287–301, 1998.

[23] D. Geldart, E. C. Abdullah, A. Hassanpour, L. C. Nwoke, and I. Wouters, "Characterization of powder flowability using measurement of angle of repose," *China Particuology*, vol. 4, no. 3-4, pp. 104–107, 2006.

[24] M. A. Kaleem, M. Z. Alam, M. Khan, S. H. I. Jaffery, and B. Rashid, "An experimental investigation on accuracy of Hausner Ratio and Carr Index of powders in additive manufacturing processes," *Metal Powder Report*, vol. 76, pp. 1–5, 2020.